ACS APPLIED MATERIALS & INTERFACES

Research Article

www.acsami.org

Thermo-cross-linked Elastomeric Opal Films

Christian G. Schäfer,[†] Benjamin Viel,[‡] Goetz P. Hellmann,[†,‡] Matthias Rehahn,*[,†] and Markus Gallei*[,†]

[†]Ernst-Berl Institut für Technische und Makromolekulare Chemie, Technische Universität Darmstadt, Alarich-Weiss-Straße 4, D-64287 Darmstadt, Germany

[‡]Deutsches Kunststoff-Institut, Schlossgartenstrasse 6, D-64289 Darmstadt, Germany

Supporting Information

ABSTRACT: An efficient and convenient thermal cross-linking protocol in elastomeric opal films leading to fully reversible and stretch-tunable optical materials is reported. In this study, functional monodisperse core−shell particles were arranged in a face-centered cubic (fcc) lattice structure by a melt flow process. A problem up to now was that un-cross-linked films could not be drawn fully reversibly and hence lost their optical and mechanical performance. After thermal cross-linking reaction, the obtained films can be drawn like rubbers and the color of their Bragg reflection changes because of controlled lattice deformation, which makes the cross-linked films mechanochromic sensors. Different techniques were developed for the cross-linking of the films a posteriori, after their preparation in the melt flow process. A photo-cross-linking approach was reported earlier. This study now deals with a very efficient thermo-cross-linking approach based on the chemistry of hydroxyl- and isocyanate-functionalities that form urethane bridges. The focus of the present work is the mechanism and efficiency of this cross-linking process for elastomeric opal films with excellent mechanical and optical properties.

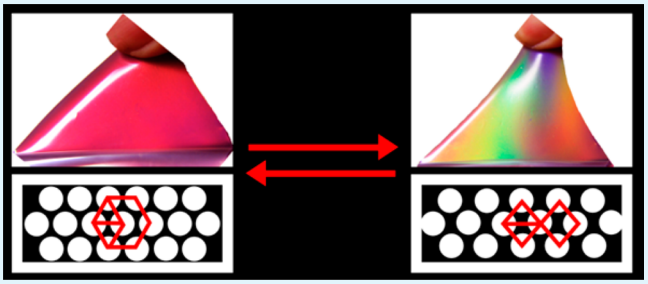

KEYWORDS: *emulsion polymerization, cross-linking, self-assembly, photonic crystals, elastomers*

INTRODUCTION

The colloidal crystallization of monodisperse particles is known as an attractive and inexpensive method leading to photonic band gap materials for a manifold of optoelectronic applications.[1−8] Thus obtained structures feature a remarkable optical performance with iridescent reflection colours caused by the Bragg diffraction of visible light.[9−17] A recent review dealing with self-assembled photonic materials is given by López et al.[18] Synthetic opals consist of monodisperse submicroscopic particles arranged in a face-centered cubic (fcc) lattice. Various strategies exist to obtain highly ordered 3D arrays based on colloid spheres, e.g., sedimentation in a force field, colloidal crystallization driven by repulsive electrostatic interactions, and in particular, the template-directed preparation of macroporous materials.[1,16,19,20] However, large-scaled opals are normally prepared by drying[21−23] or spin coating[24,25] of dispersions of their particles but they can also be prepared in the flow fields of confined melts: the melt-flow technique, involving the compression of the particles between the plates of a press, permits the preparation of large-area self-supporting opal films.[17] The promising melt-shear organization technology, for which core−shell particles consisting of a rigid core and a soft, elastomeric shell are essential, was developed over the last decade.[26−28] In contrast to other preparation processes like drying or spin coating, large-area and crack-free films can be produced by this technique, which combines extrusion, rolling, and subsequent edge-induced rotational shearing to produce large-area elastomeric opal films.[29−31] As all opals, these melt-flow films reflect angle dependent colours corresponding to Bragg's law. Remarkably, such films are able to show their color change by controlled stretch-induced lattice deformation making these films very attractive for a wide range of large-area photonic and optical sensor applications.[32−34] Because the strain deforms the fcc lattice, the deformed film can reflect all colors of the rainbow, making these films potential candidates for mechanochromic devices. As in most opals, the (111) plane of the fcc lattice extends parallel to the film surface with the period a_{111}. As white light is shone on the opal, the lattice reflects a colour with the Bragg wavelength

$$\lambda_{111} = 2na_{111}\sin\delta \quad (1)$$

which depends on the average refractive index n, the angle δ of the light path inside the film, and the period a_{111}. As the film is drawn to a strain ε, this period decreases to a_ε and with it the reflected wavelength λ_ε leading to a blue-shift of the reflection

$$\lambda_\varepsilon/\lambda_{111} = a_\varepsilon/a_{111} \quad (2)$$

It has been reported earlier that at a certain strain ε^*, the lattice is rotated: above ε^*, the *hkl* plane extending parallel to the film surface is no longer (111), but (200).[17,33] To obtain such

Received: July 1, 2013
Accepted: October 17, 2013
Published: October 17, 2013

mechanochromic film disks, hard-soft core-shell particles were heated in a press to melt the shells, then the melt was squeezed under pressure and forced to flow outwards between the plates. Under these conditions, the melt flows in a parabolic flow field in which it crystallizes successively. But a problem with these mechanochromic films so far is that while applying higher strains, the film deformation cannot be assumed to be fully reversible as the particles are not chemically interconnected to a coherent network, which is essential for true elasticity. On the other hand, the films must be uncross-linked while they are crystallized in the melt, otherwise they would not flow. Hence, a premature cross-linking would hinder or even completely prevent the melt-flow structuring which is essential for the opalesque crystallization. For this reason, cross-linking processes are necessary that reliably do not proceed under the conditions of crystallization but can be activated a posteriori. An in situ cross-link network, generated by subsequent UV irradiation of the melt-flow opal films, proved earlier to enhance the mechanical and optical properties of the opal films considerably. Here, films containing added benzophenone were radically photocross-linked (Scheme 1, top).[33] However, above a certain film thickness (above 200 μm), the photocross-linking reaction remained incomplete. To the best of our knowledge, an in situ thermo-cross-linking protocol for elastomeric opal films has not been applied up to now. Thermally induced cross-linking would enable the preparation of even thicker films with enhanced mechanical properties.

Scheme 1. Conceivable Cross-Linking Reactions of Core−Shell Particles with Different Chemical Composition: Photochemical Cross-linking Reaction with Benzophenone (top)[33] or Thermal Cross-linking with Diisocyanates (bottom)

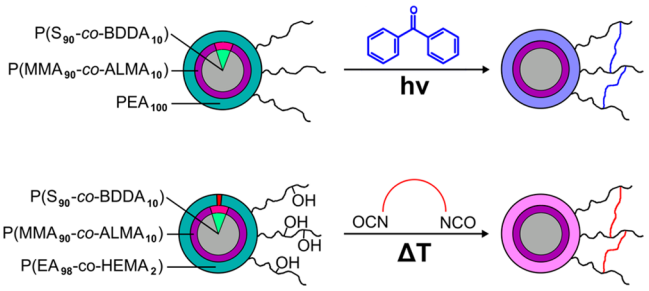

In the present study, we address films with hydroxyl functions in the shells of the monodisperse particles which can be cross-linked with added (oligo)isocyanates (Scheme 1, bottom) simply by heating the film. Blocked oligoisocyanates (Crelan UI and Crelan EF403, Bayer AG) were employed as cross-linkers that de-block at high temperatures.[35−41] After the de-blocking reaction, the isocyanate moieties can couple easily with alcohols to form cross-linked elastomeric opal films with remarkable reflection colours. These novel thermocross-linked elastomeric opal films are investigated with respect to their mechanical and excellent optical properties and they open access to a large family of easily scalable and adjustable mechanochromic sensors.

EXPERIMENTAL SECTION

Materials. Styrene (S), ethyl acrylate (EA) and butanediol diacrylate (BDDA) were obtained from BASF SE, allyl methacrylate (ALMA) and methyl methacrylate (MMA) from Evonik Röhm GmbH and hydroxyethyl methacrylate from Acros. The blocked isocyanate cross-linkers Crelan UI (UI) and Crelan EF403 (EF) were obtained from Bayer Materials Science. All other chemicals were purchased from VWR and Sigma Aldrich and used as received. Prior to use in the emulsion polymerization, the stabilizers 1,4-dihydroxybenzene monomethylether and 1,2-dihydroxybenzene monomethylether were removed from the monomers. Therefore, EA was extracted with 1 N sodium hydroxide solution, washed with water until the solution was neutral followed by drying with sodium sulfate. S was distilled under reduced pressure. ALMA and BDDA were destabilized by an ion exchanger (De-Hibit 200, PolySciences Europe GmbH). For use in emulsion polymerization, deionized water was bubbled with nitrogen for at least 30 min. For the coagulation of the latices, technical grade methanol and sodium chloride were used. The Crelan products (Bayer) were used without further purification after grinding in a laboratory mill.

Synthesis of PS_{PMMA}-co-PEA_{HEMA} CIS Particles. Under argon a 1 L flask equipped with stirrer and reflux condenser was filled at 75 °C with a cold monomer emulsion of 217 g of deionized water, 0.40 g of BDDA, 3.6 g of S, and 0.180 g of sodium dodecylsulfate (SDS). Subsequently, the polymerization was initiated by adding 50 mg of sodium bisulfite, 350 mg of sodium peroxodisulfate (SPS), and 50 mg of sodium bisulfite in this sequence (PS seed). After 10 min, a monomer emulsion consisting of 6.6 g of BDDA, 59.4 g of S, 0.300 g of SDS, 0.1 g of KOH, and 90 g of deionized water was added continuously over 100 min (PS core). After 10 min, 100 mg of SPS was added. After an additional 10 min, a monomer emulsion consisting of 3.0 g of ALMA, 27.0 g of MMA, 0.150 g of SDS, and 40 g of water was added continuously within 45 min (PMMA interlayer). After 10 min, a monomer emulsion of 130.0 g of EA, 2.6 g of HEMA, 0.330 g of SDS, and 139 g of water was added continuously over 180 min (PEA_{HEMA} shell). During the polymerization samples were taken and dried on glass slides where the particles always formed a coloured opal layer. The red-shift of the colour indicated the increasing diameter D of the particles. Particles as specified by the above recipe revealed an overall diameter of $D \cong 300$ nm when prepared with exactly 0.180 g of the surfactant SDS in the seed stage. Other diameters were obtained by changing slightly the amount of SDS. These particles had the following composition: $w_{core}:w_{interlayer}:w_{shell}$ = 30:13:57 wt %.

Compression Molding. For preparation of the opal films, the latices (containing 30 wt % polymer) were coagulated in methanol, filtered and dried. The elastomeric mass was mixed with 3 wt % of a Crelan cross-linker, 0.3 wt % wax (Licolub FA1, Clariant) and 0.1 wt % of carbon-black powder (N990, Freudenberg) in a microextruder (micro1, DSM Research) at 120 °C. The components always formed homogeneous mixtures. 4 g of the extrudates were then heated to 120 °C between the plates of a laboratory press (300E, Dr. Collin), which were covered with polyethylene terephthalate (PET) foil. Then, melt flow was induced with a pressure of 50 bar. The melt was not confined in a cavity but was allowed to flow freely sideways. After 1 min, the film was allowed to cool to room temperature. Film disks typically show 300 μm thickness and a diameter of 12 cm. For the thermal cross-linking, the PET foil on the top of the opal films was removed and the films were transferred into an oven at 190 °C, where they were cured for 5 min or 10 min, respectively.

Characterization Methods. ^{1}H NMR spectra were recorded on a DRX 500 NMR spectrometer (Bruker) working at 500 MHz. NMR chemical shifts are given relative to tetramethylsilane. The AFM measurements were performed on a CP-II atomic force microscope (Veeco) in contact mode with a silicon cantilever MPP 21123-10, k = 3 N m^{-1}(Veeco). The lateral deflection frequency was 1.2 Hz. Reflection spectra were recorded using a Lambda 900 UV/vis spectrophotometer (Perkin Elmer). Reflection measurements as a function of strain ε were carried out at normal light incidence. Therefore, a 1 × 2 cm^2 strip of the films was uniformly stretched with a custom-made micrometer-controlled sample holder, while the optical properties were measured simultaneously. The deformation of the samples was characterized in a tensile tester Z020 TH2A (Zwick), using dog bones that were cut from the film disks in the radial direction. Single stress−strain tests up to the tearing point were

performed with a strain rate of 15% min^{-1} as well as strain-and-release cycles to a defined maximum elongation. Thermal properties were characterized using a differential scanning calorimeter (DSC) Mettler-Toledo DSC822 equipped with a TSO801R0 autosampler. A scan rate of 10 K min^{-1} was employed. Standard SEC was performed with THF as the mobile phase (flow rate 1 mL min^{-1}) on a Mixed Gel column set from PL (PL Mixed Gel B, PL Mixed Gel C, PL Mixed Gel D) or an SDV column set from PSS (SDV 1000, SDV 100000, SDV 1000000) at 30 °C and a refractive index detector RI 410 (Waters). Calibration was carried out using polystyrene (PS; from Polymer Standard Service (PSS), Mainz)

Kinetic Studies. The kinetics of the urethane formation was studied in model reactions. For that purpose, isophorone diisocyanate (IPDI) or one of the Crelans used were fed together with the alcohol dodecanol into glass ampules without a solvent. The two components always formed homogeneous mixtures. The consumption of the dodecanol was measured using the CH signal of the $-CH_2OH$ group in the unreacted alcohol in the ^1H NMR spectrum at $\delta = 3.7$ ppm. The system with IPDI was also investigated by using size-exclusion chromatography (SEC). The de-blocking reaction of the neat Crelans was recorded with DSC at a heating rate of 10 K min^{-1}.

RESULTS AND DISCUSSION

Synthesis and Processing of Core-Interlayer-Shell (CIS) Particles. Monodisperse CIS particles featuring rigid cores and surface-anchored soft elastomeric shells were synthesized by using semi-continuous and stepwise emulsion polymerization as described in the Experimental Section. The chemistry, size and architecture of the particles were optimized as follows: Firstly, the core size was adjusted by using emulsion polymerization protocols to obtain particles of 170 nm to 200 nm size. These sizes allow the preparation of opal films with reflection colours ranging from green to red under normal light incidence (θ = 90°). Secondly, the ratio of the hard core (including the interlayer) and the soft shell was fixed at ≅ 43:57 which proved to guarantee good crystallization in the melt (Scheme 1, bottom). Additionally, it was important that the core and the shell have a sufficient refractive index contrast of $\Delta n \cong 0.1$ for bright colours, so polystyrene (PS) (n = 1.59) was chosen for the core and polyacrylates for the shell ($n \cong 1.48$). Moreover, it was necessary to cross-link the PS cores sufficiently to keep their shape at all temperatures and strain conditions used. The shell consisted of poly(ethyl acrylate) (PEA) revealing a glass transition temperature of −20 °C. Hence, the films had the consistency of a soft solid at room temperature enabling the material to flow in the press at 120 °C. But nevertheless the films were able to keep their shape during the curing step even at a temperature of 190 °C. For the curing reactions with the isocyanates, the particle shell was functionalized with hydroxyethyl methacrylate (HEMA) comonomer that provided the required hydroxyl moieties for intended urethane formation with isocyanates (Scheme 1, bottom).

The particle architecture allows the preparation of polymer opal films with the intrinsic capability for subsequent cross-linking reaction after their preparation in the melt. A full description of the process is given in the Experimental Section. During the uniaxial compression at elevated temperature, the molten elastomeric mass freely flowed sideward and the cores arranged themselves in the flowing melt into stacked hexagonal layers resulting in a precise fcc arrangement of hard PS cores embedded in soft polyacrylate matrix. Hence, (111) planes of the fcc lattice were parallel aligned to the prepared film surfaces. The resultant opal film revealed a brilliant and distinct red iridescent reflection color (Figure 1, left). The precise arrangement of the surface parallel (111) planes could be proven by AFM investigations of the corresponding film surface (Figure 1, right).

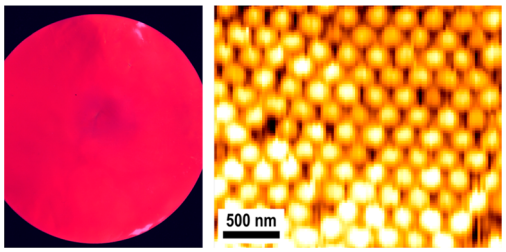

Figure 1. Photograph of the film disk (12 cm diameter) showing the strong red reflection color (left) and AFM image of the surface of elastomeric opal film prepared showing the hexagonally ordered (111) plane (right).

The final samples were disks of elastomeric polymer opal films with a diameter of 12 cm and a thickness of around 300 μm. Hexagonally arranged PS cores (light) embedded in a PEA matrix (dark) were clearly visible in the AFM image (Figure 1, right) demonstrating that highly ordered opal films are accessible from these hydroxyl functionalized particles. It has to be borne in mind that grafting the PEA shell onto the PS core was necessary for applied procedures. This core/shell connection was guaranteed by forming an allyl methacrylate (ALMA) cross-linked poly(methyl methacrylate) (PMMA) interlayer between the polystyrene (PS) core and the PEA shell (Scheme 1, bottom). Without grafting, the films did not crystallize in the melt. In another study of silica/acrylate-based particles with the same PMMA interlayer, the optimal degree of shell grafting could be determined: it is necessary to graft one third of the shell chains.[42] An analysis of the films of the present study proved that the films consisted of CIS particles PS/PMMA/PEA by 30 + 13 + 37 ≅ 80 wt %. The remainder of 20 wt % are loose, unconnected PEA chains that form a matrix around the particles (Figure 2a). From the SEC trace in Figure

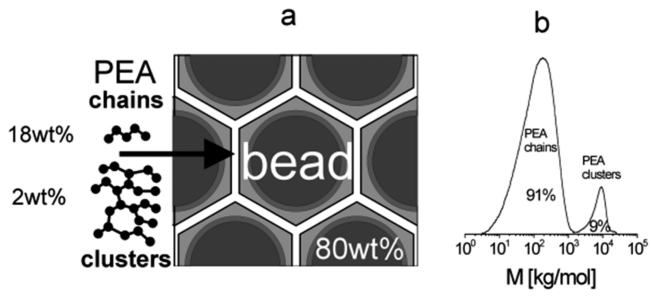

Figure 2. (a) Composition of the elastomeric opal film and (b) SEC trace of the isolated matrix material for determining the matrix composition.

2b, it can be concluded that this PEA matrix had a bimodal molar mass distribution: it consisted of single PEA chains and clusters thereof, with molar masses of 100 kg mol^{-1} and 1×10^4 kg mol^{-1}, respectively.

Branching reactions in polyacrylate syntheses derive from the reactions with the α hydrogens. Hence, 20 wt % of the whole film consisted of a PEA matrix with 18 wt % linear and 2 wt % branched chains. Hence, an opal film consists of three components differing significantly in size: the particles as well as the branched and the linear PEA chains. For a coherent

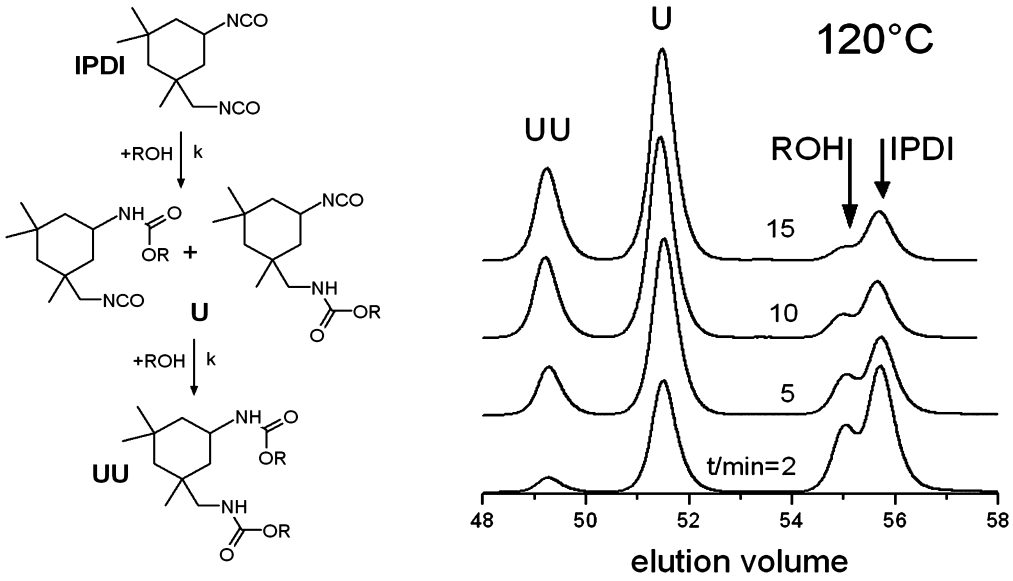

Figure 3. Model reaction of isophorone diisocyanate (IPDI) with an alcohol (dodecanol, R−OH) for the urethane formation (left) and SEC elugrams of reaction aliquots taken after 2, 5, 10, and 15 min (right). U denotes the reaction of a single NCO group with the alcohol (mono-urethane), whereas UU denotes the di-urethane formation.

network of any polymer system, at least two cross-link points per unit are necessary to make the film elastic. Assuming an opal film with an amount x of hydroxyl moieties (from the HEMA) and a stoichiometric amount of isocyanates, the number of the hydroxyl functions per unit (particle, cluster or chains) is given by xP, where P is the degree of polymerization of the unit. The number n_{XLINK} of cross-linking points, which must exceed the value of 2, is given by xP and the conversion C_{XLINK} to urethane cross-link points:

$$n_{XLINK} = C_{XLINK} xP \geq 2 \quad (3)$$

The conversion C_{XLINK} and its consequences for the performance and the elasticity of the opal films are described in the following. Direct analysis of the cross-link network in the opal films was impossible. Hence, the kinetics of the isocyanate-hydroxyl coupling to urethane cross-links was measured in model systems as described in the following section.

Model Studies of the Urethane Formation. The kinetics of the urethane formation was investigated by using SEC measurements and ^{1}H NMR spectroscopy. As model system for the urethane formation in the opal films, the reaction of isophorone diisocyanate (IPDI) with dodecanol without using a solvent was studied (Figure 3, left). IPDI bears a cyclic and an acyclic isocyanate (NCO) functionality slightly differing with respect to their reactivity.[43−47] SEC traces obtained for aliquots of the reaction after 2, 5, 10, and 15 min at 120 °C reaction temperature are given in Figure 3 (right).

From Figure 3, it can be concluded that besides the signals for the unreacted IPDI and dodecanol, two peaks emerged with prolonged reaction time: These two peaks can be assigned to the mono-urethane (U) and the di-urethane addition product (UU). The evaluation of the SEC peaks led to conversion curves at 190 °C reaction temperature as shown in Figure S1 (left) in the Supporting Information. The kinetic of the polyurethane formation is described in more detail in the Supporting Information. Kinetic investigations are important for two reason: first, to verify that a second-order kinetic model describes the urethane formation adequately,[47] and second, to establish that the reaction is fast and efficient at 190 °C. Unfortunately, analogous SEC measurements were impossible with the Crelans used due to their oligomer distribution. Instead, the reaction of the Crelans UI and EF403 and - for comparison - IPDI with dodecanol was followed using ^{1}H NMR spectroscopy by measuring the alcohol consumption in 1:1 mol % mixtures for C_{NCO} and C_{OH}. Conversion curves for all three reactions with dodecanol at 190 °C are given in Figure 4.

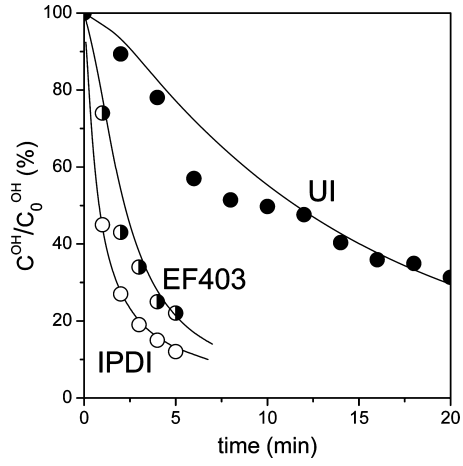

Figure 4. Conversion of the isophorone diisocyanate (IPDI), Crelan UI ($c_{OH(t=0)}$ = 1.9 mol kg^{-1}) and Crelan EF403 ($c_{OH(t=0)}$ = 3.4 mol kg^{-1}) with a dodecanol at 190 °C.

The curves in Figure 4 were fitted with the kinetic model, which is described in detail in the Supporting Information. As can be extracted from Figure 4, the experimental data obtained from the IPDI model reaction are in very good agreement with the kinetic model. However, the two different Crelans reacted significantly slower than IPDI because of the preceding deblocking reactions for the isocyanate functionalities (Scheme 2).

The sequence modelling from the blocked isocyanate (bNCO) over the free isocyanates (NCO) and finally to the

Scheme 2. Preceding Deblocking Reaction of the Crelans UI and Crelan EF403 Leading to the Free Isocyanate Functionalities (NCO) That Were Able to React with Added Alcohol (ROH, dodecanol)[a]

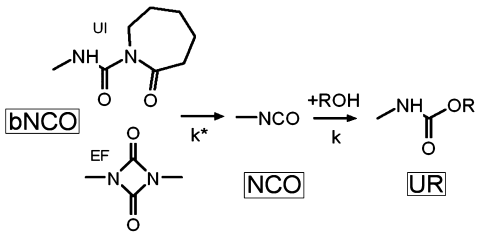

[a] k^* is the first-order rate constant, whereas k denotes the second-order constant (eq 7).

urethane (UR) can be derived as described in the Supporting Information. From these calculations, the curves C_{OH} in Figure 4 for the Crelans were fitted with $r \cong 0.5$ for Crelan EF403 and $r \cong 0.1$ for Crelan UI because of the faster deblocking reaction of Crelan EF403 compared to Crelan UI. This behaviour was also confirmed by thermo-analytical studies: the exothermic peaks in the DSC traces of the pure Crelans (Figure 5) caused

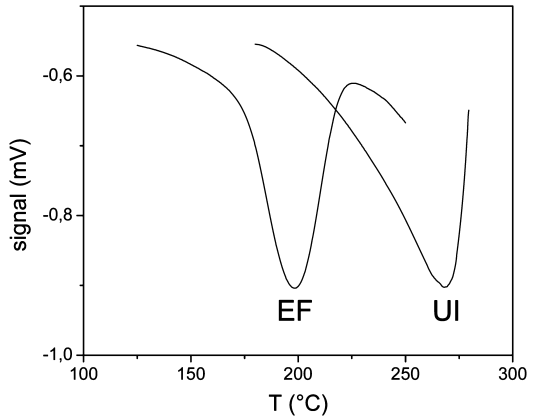

Figure 5. DSC thermograms for pure Crelan EF403 and Crelan UI.

by deblocking reaction, revealed that EF403 reacted at a lower temperature than UI. The peak maximum indicated a half-life time of $t_{1/2} \cong 1$ min at 192 °C for Crelan EF403, whereas for Crelan UI, the same half-life time value could be obtained at 255 °C. This is an important information for comparison of the different Crelans used and thereby the thermally induced cross-linking reaction efficiency.

Predictions on the Cross-linking Reactions. In the opal films, the hydroxyl functions of the HEMA comonomer in the shells of the particles were supposed to couple with the isocyanate functions of IPDI or the Crelans used to build up a thermally induced urethane cross-link network. The knowledge about the amount of cross-links inside the opal films could not directly be measured and has to be calculated from the results of the model studies (cf. Supporting Information). The opal films contain only a small amount of HEMA in the PEA shell as too many OH functions unduly increased the viscosity of the films. However, the few OH functionalities were supposed to lead to an elastic network within 10 min at 190 °C as determined by the important model reactions. Empirically we found that cross-linking succeeded best with a content of HEMA of x_{HEMA} = 2 mol %. Films with fewer OH functions were too soft and films with a high content of HEMA were too hard and brittle. Hence, only the mechanical and optical properties for films obtained by melt compression from particles with PS_{PMMA}-*co*-$PEA_{HEMA(2\%)}$ will be discussed.

The kinetics were calculated from the model study discussed above (with C_{NCO}:C_{OH} = 1:1). The films differed from the model systems with respect to the viscosity and the concentration of the NCO and OH functions. The viscosity was not significant for the reaction kinetics as the reaction was not diffusion-controlled. Instead, the content of NCO and OH moieties was much more important: the model systems were very concentrated, with $c_{OH(t=0)}$ = 3.4 mol kg^{-1} in the Crelan EF403 and 1.9 mol kg^{-1} in the Crelan UI system. On the contrary, the opal films contained OH and NCO functionalities of approximately $c_{OH(t=0)}$ = 0.19 mol kg^{-1}. The significant dilution retards the cross-linking reactions. But however, this effect is not linear: a lower $c_{OH(t=0)}$ did not change the first-order deblocking reaction, it only slowed down the second-order urethane formation (Scheme 2). The calculated kinetics for the thermally induced cross-linking reaction in the opal films are shown in Figure S2 in the Supporting Information. There, the curves C_{UR} (=1 − C_{OH}) demonstrate that both cross-linkers react at 190 °C with high conversions within 1 h

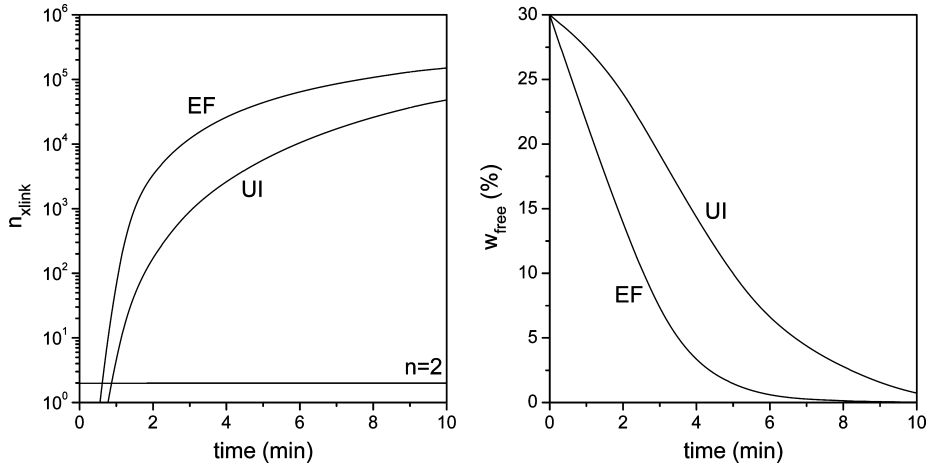

Figure 6. Contribution to the network formation of the reagents in the opal films: number of cross-links n_{XLINK} per particle (left) and fraction of the ungrafted PEA matrix w_{free} that does not participate to the network formation (right).

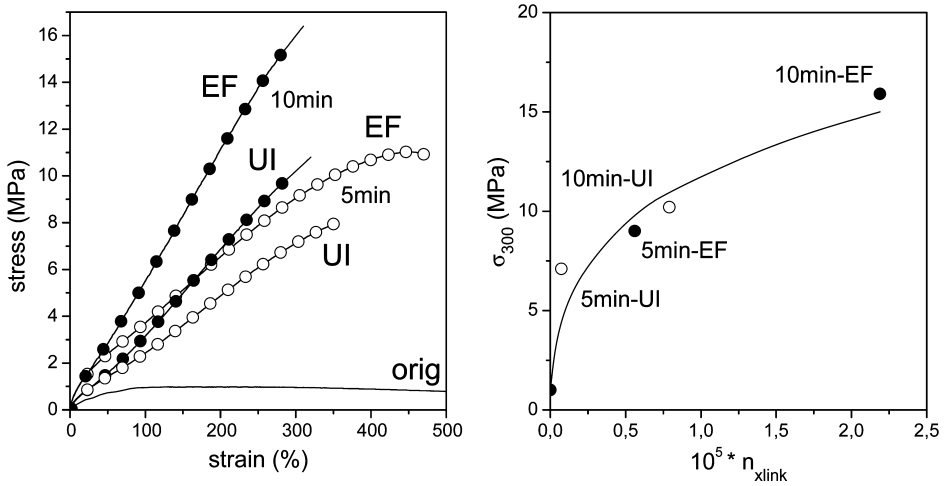

Figure 7. Mechanical properties of the opal films: stress−strain curves (left) and stress σ_{300} at a strain of ε = 300 % as a function of the number n_{XLINK} of cross-link points of the particles (right).

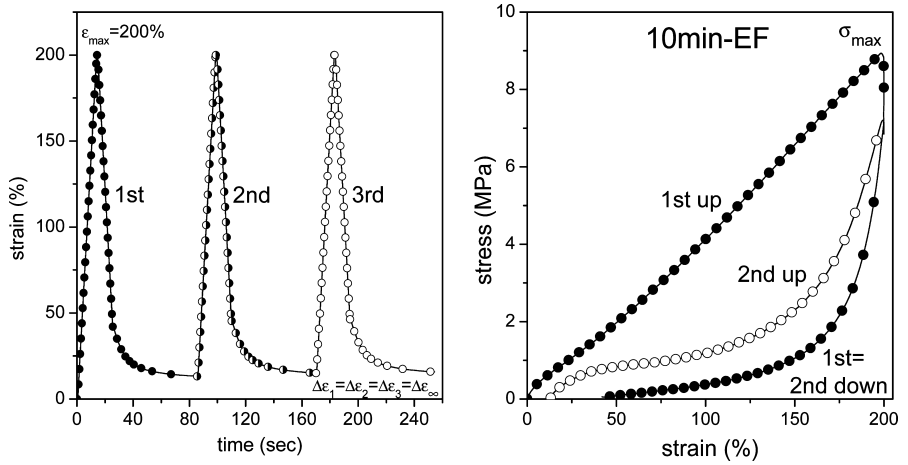

Figure 8. Mechanical tests (up-down-wait cycles) for a film cured with Crelan EF403 for 10 min: strain-time protocol (left) and stress−strain curves (right). $\Delta\varepsilon_1$ denote the end of the waiting period.

and that Crelan EF403 reacts faster than Crelan UI. However, the concentration C_{UR} as such is not very informative. The network in the opal films is characterized much better by two other parameters: the cross-link density and the as yet uncross-linked PEA matrix. The cross-link density is related to the C_{XLINK} curves in Figure S2 in the Supporting Information, which indicates how many OH functions as part of the P(EA-*co*-HEMA) chains participate in cross-linking reactions. Because the molar masses of the reagents that are able to participate in cross-linking reactions are $P_{chain} \cong 1 \times 10^3$, $P_{cluster} \cong 1 \times 10^5$, and $P_{shell} \cong 1 \times 10^7$, the cross-linking between the shells will dominate. That means that the particles will be directly connected to the network. The number of cross-links n_{XLINK} on these particles increases rapidly with C_{XLINK}: even if only the presence of grafted PEA clusters, which make $f^* \cong 7\%$ of the total PEA, were assumed to protrude enough from the shells to form cross-links between particles, the minimum $n_{XLINK} = 2$ for a complete particle-to-particle network is surpassed easily because

$$n_{XLINK} = f^* x P C_{XLINK} \cong 1 \times 10^4 C_{XLINK} \quad (4)$$

The curves in Figure 6 (left) based on eq 4 show that the particles indeed carry a high number of cross-links even after a few minutes reaction time, although the concentration of cross-links C_{XLINK} was still very low in this early stage of the reaction.

The ungrafted PEA chains and clusters only marginally participate in the network formation. During the urethane formation, they are supposed to be attached to the particle network as dangling ends. The PEA chains that are not connected to the network are dominated by the short PEA chains which represent $f \cong 30\%$ of the total amount of PEA. During the reaction, the content of still free PEA chains decreased. As shown in Figure 6 (right), this share vanished after 10 min curing time indicating that the opal films contained no mobile PEA anymore. But after 5 min in the Crelan UI cured films, about one third of the original PEA matrix were still free so the network of the particles can be assumed to float into the mobile matrix. The effects on the mechanical properties are discussed in the following.

Tensile Behavior of the Opal Films. For investigations of the mechanical performance of the elastomeric material, opal films cured for 5 or 10 min with the Crelan UI or EF403 were characterized in a tensile tester. Corresponding tensile curves are given in Figure 7 (left).

The uncured film free of cross-links was soft as a rubber, but it did not behave like an elastomer. It could be drawn on a

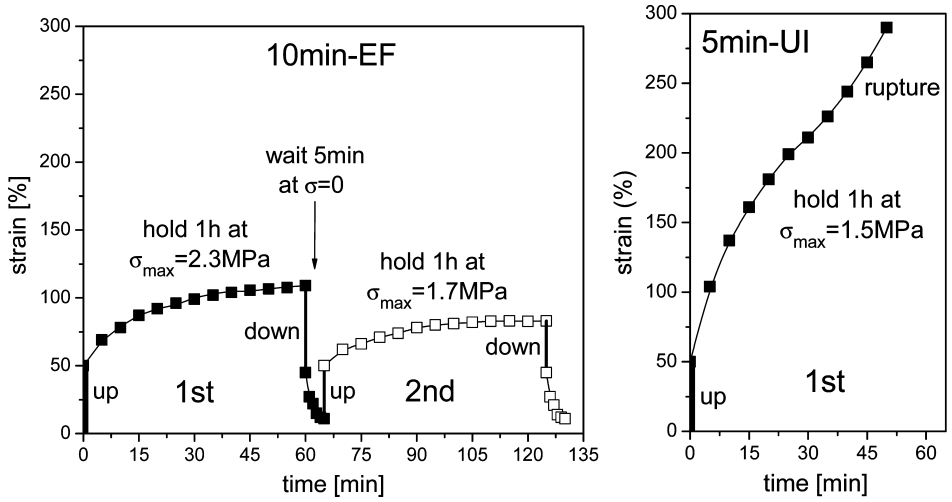

Figure 9. Results of the up−hold−down−wait cycle experiments for a 10 min cured Crelan EF403 film (left) and a 5 min cured Crelan UI film (right).

stress level <1 MPa almost indefinitely, which classified it as viscous liquid. On the other hand, the cross-linked films were much stiffer. They can be deformed in length for several times as function of a steadily increasing stress up to $\sigma \cong 10$ MPa. The values at break were higher after a longer curing time of the opal films revealing that Crelan EF404 was the more efficient cross-linking reagent. In Figure 7 (right) the stress σ_{300} (at $\varepsilon = 300$ %) as a measure of the film stiffness was correlated with the number of cross-links n_{XLINK} between the particles. As to be expected, the first cross-links increased the hardness particularly strong. Because these simple stress−strain curves provided no information about the quality of elasticity, cyclic mechanical tests were carried out (Figure 8). Common tests therefore are up-down tests where the stress is recorded in a (repeated) draw-and-release cycle. This study reveals hysteresis effects. This experiment is even more informative, when some waiting time at $\sigma = 0$ is added allowing the film to relax (up-down-wait cycles). But the most discriminative cyclic test has an up-hold-down-wait programme in which the film is held between the up and down stage for some time at the stress σ_{max}. This time under stress activates the flow in the film immensely. Up-down-wait cycles to a maximum strain of $\varepsilon_{max} = 200\%$ are shown in Figure 8 for a film (cured with Crelan EF403 for 10 min) which was drawn and released at a constant strain rate (15 % min^{-1}) and then kept (1 min) in the stress-less state before the second cycle was carried out. The film did not fully retract immediately after release but stopped at a residual strain of $\Delta\varepsilon = 36$ %. At first glance, a permanent damage could be assumed caused by the deformation but it turned out that this was only a transient phenomenon. The film relaxed in the waiting period to a very small permanent strain $\Delta\varepsilon_1 = \Delta\varepsilon_\infty = 11$ % in the first cycle and 13% in following cycles. This indicated satisfactory elasticity.

Nonetheless the stress-strain curves in Figure 8 (right) look rather like those obtained for a thermoplastic elastomer (TPE)[48] demonstrating that the film do not behave like an elastic rubber. The first up curve is far above the down curve. The system turned the part of its acquired mechanical energy into heat. This hysteresis was very similar to that observed for TPE. All other TPE characteristics were obvious as well: the second up curve was below the first, the second down curve equaled the first, the heat Q in the second cycle was small and all further cycles were practically equal to the second. This kinship to TPEs may be owed to a similar structure: both the opal films and TPEs consist of hard microphases in a soft matrix. Unfortunately, the up-down-wait programme yielded approximately the same results for all films tested. In summary, the permanent deformation was rather small, $\Delta\varepsilon_\infty < 20\%$. The disadvantage of the cyclic test used was that the films were not tested for their ability to sustain permanent stress. Hence, up-hold-down-wait cycles up to a strain of $\varepsilon_{max} = 50\%$ were carried out. During a long holding period of 1h at the maximal stress σ_{max}, the films had to prove their elasticity under rather harsh conditions. Indeed, this test revealed the differences in elasticity: a film cured for 5 min with Crelan UI and a film cured with Crelan EF403 for 10 min are shown in Figure 9. The 10 min-cured EF film contained a network with an order of magnitude denser than the 5 min-cured UI film. The 5 min-cured UI film still contained a free PEA matrix compared to the EF film.

From Figure 9 it can be concluded that the EF403 film crept in the 1st cycle during the holding time to about twice its length eventually reaching equilibrium. This behaviour characterizes a rubber with a stable cross-link network that can withstand stress, albeit after some creep probably due to network inhomogeneities. This film relaxed after the down and wait period to approximately $\Delta\varepsilon_\infty = 11$ % of permanent strain. The changes in the second cycle were reminiscent of Figure 9: the maximum strain was decreased and the creep at σ_{max} was less pronounced. All these phenomena confirmed that this film contained a strong cross-linked network. However, the 5 min-cured Crelan UI film was not stabilized by a sufficiently strong network. As shown in Figure 9 (right), the film crept or rather flowed like a viscous liquid in the first holding period until it ruptured. Apparently, a great number of cross-links was needed to stabilize the network between the particles.

In summary, the up-hold-down-wait mechanical test program allowed a good distinction between the mechanical performance of the opal films. The tested films were not perfectly elastic but the 10 min-cured Crelan EF403 film revealed a good cross-link network, which enabled this film to sustain permanent stress while the UI-cured failed.

Optical Properties of the Films. The formation of a stable elastomeric structure could be achieved for the 10 min-cured

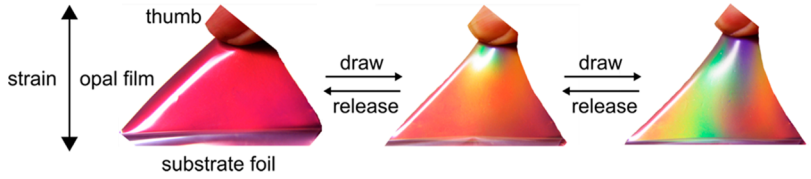

Figure 10. Crelan EF403-cured elastomeric opal film and accompanied reflection color changes by applying strain.

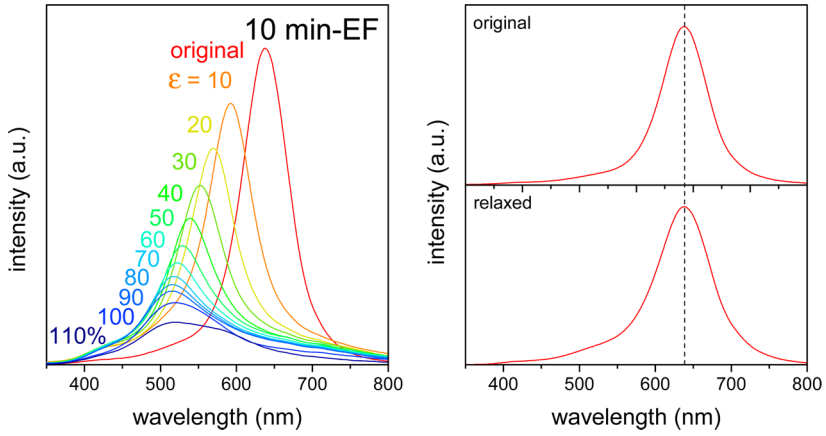

Figure 11. Strain-dependent UV/vis reflection spectra of the 10 min cured Crelan EF403 film (left) and comparison of reflection spectra of the original film and the film after relaxation (right).

Crelan EF403 film showing a good mechanical performance in the mechanical tests. As expected, the thermally induced cross-linking reaction led to elastomeric polymer opal films with an almost rubber-like behavior which is the basic prerequisite for a completely reversible film deformation. As the cross-linked opal films feature an elastomeric behavior, the color of the films can be switched under strain due to a controlled lattice deformation changing both the symmetry and the spacing of the lattice. As demonstrated in the photograph in Figure 10, applied strain causes a blue shift of the reflection color through the whole visible spectrum from initial red to blue.

Strain-induced reversible tunability of the optical stop band and the 3D structure changes in the polymer opal fcc lattice were characterized and directly compared to the results of the up-hold-down-wait cycle experiments in Figure 9. The shift of the stop band while applying strain up to levels of $\varepsilon > 100\%$ was characterized by using UV/vis spectroscopy in reflection under normal incidence at the same spot of the stretched sample (Figure 11, left). The reflection measurements of the original film ($\varepsilon = 0\%$) compared to the film after stretching above $\varepsilon > 100\%$ and subsequent relaxation are additionally shown in Figure 11 (right).

The stop band corresponding to the surface parallel (111)-lattice planes generates a Bragg peak at λ=635 nm corresponding to the lattice plane spacing of stacks of the hexagonally arranged PS cores in the highly ordered fcc lattice (Figure 11, left). The blue-shift of the (111) plane stop band was clearly visible in reflection spectra, as the strain was increased from 0 to 90%, whereas the intensity decreased significantly (Figure 11, left). The spectra featured a Bragg peak due to selective backward scattering from the (111) planes of the fcc lattice which shifted upon film elongation to shorter wavelengths caused by both decreasing the spacing and changing the symmetry of the (111) planes. The structural transitions inside the elastomeric polymer opal films under deformation were addressed in a previously published work.[33]

Notably, at strains of $\varepsilon \geq 100\%$ the Bragg peaks vanished and no reflection from the (111) lattice plane could be observed in the reflection spectra (Figure 11, left). To sum up the spectral features assuming elastomeric behavior of the films, strain induces a significant blue shift of the reflected color, which is accompanied with a tremendous photonic band gap shift of about 120 nm. But because of the elastomeric feature obtained for the thermally induced cross-linked matrix, this process is now completely reversible. After relaxation, the film revealed inverted color shifts and the original opal structure was totally restored after typically less than 1 min. This is evidenced by studying the initial optical properties—with the Bragg peak positioned at λ = 635 nm (Figure 11, right, top)—and comparing the results with the relaxed film (Figure 11, right, bottom). This result impressively demonstrates that the photonic band gap shift of these films in strain-and-release cycles is fully reversible because of their elastomeric properties, which can be utilized, for example, in strain sensor applications. Similar studies were carried out for the Crelan UI-cured elastomeric opal film (see the Supporting Information, Figures S3−S5). Applied strain shifts the peak position so efficiently that a light source emitting at λ_{111} can already be switched on and off in draw-and-release cycles up to rather weak strains of $\varepsilon \cong 10$ %. At these weak strains, all opal films were perfectly elastic, without a hysteresis and a permanent residual strain $\Delta\varepsilon_{\infty}$. In summary, the 10 min-cured Crelan EF403 film should be most feasible for optomechanical devices.

CONCLUSION

Opal films of submicroscopic core-interlayer shell (CIS) particles with an elastomeric shell change their colour when drawn due to a strain-induced decrease of the (111) spacing in the fcc lattice. The colour change can be made reversible by cross-linking the particles in the film. In this study, the opal films were thermo-cross-linked by using added oligoisocyanates and functional comonomers bearing hydroxyl groups in the soft

shell of the monodisperse particles. Mechanical investigations revealed that the deformation of the films was reversible but not elastic: draw-and-release cycles showed a strong hysteresis with only little permanent deformation. The kinetics of the cross-linking reactions and the structure of the resulting networks were analysed in detail and correlated with the resulting properties. Therefore, cross-linking model reactions were carried out and insights into the reaction kinetics transferred to the opal film cross-linking reactions. It turned out that the network of cross-links between the particles sufficed to produce elasticity under mild conditions (strain ε<50%) as necessary for mechanochromic effects. The differences in network density emerged only under harsh conditions (strain >100%, creep under stress). The colour reflectance was characterized by using UV/vis spectroscopy at different strains. Strains of approximately 10% shifted the reflected colour sufficiently to switch the wavelength from an on- to an off-state in draw-and-release cycles making these films excellent candidates for mechanochromic devices. Studying the mechanical properties of the novel thermally cross-linked elastomeric opal films together with investigations of the excellent optical properties revealed that original iridescent reflection colors can be achieved after stretch-tuning the films.

■ ASSOCIATED CONTENT

Supporting Information

Additional data, kinetic model of the polyurethane formation of the model compounds, UV/vis spectra for the Crelan UI-cured opal film, stress−strain curve as function of the reflection wavelength, and stress−strain curve for the UI-cured opal film. This material is available free of charge via the Internet at http://pubs.acs.org.

■ AUTHOR INFORMATION

Corresponding Authors

*E-mail: m.gallei@mc.tu-darmstadt.de.
*E-mail: m.rehahn@mc.tu-darmstadt.de.

Notes

The authors declare no competing financial interest.

■ ACKNOWLEDGMENTS

We thank Merck KGaA (Darmstadt, Germany) and the Bundesministerium für Bildung und Forschung (BMBF project 13N8275, KODO) for financial support. C.S. wants to thank the Landesoffensive zur Entwicklung Wissenschaftlich-ökonomischer Exzellenz (LOEWE Soft Control) for financial support of this work.

■ REFERENCES

(1) Xia, Y.; Gates, B.; Yin, Y.; Lu, Y. *Adv. Mater.* **2000**, *12*, 693−713.
(2) Hynninen, A. P.; Thijssen, J. H.; Vermolen, E. C.; Dijkstra, M.; van Blaaderen, A. *Nat. Mater.* **2007**, *6*, 202−205.
(3) Maldovan, M.; Thomas, E. L. *Appl. Phys. Lett.* **2006**, *88*, 251907−3.
(4) Rue, R. D. L. *Nat. Mater.* **2003**, *2*, 74−76.
(5) Gonzalez-Urbina, L.; Baert, K.; Kolaric, B.; Perez-Moreno, J.; Clays, K. *Chem. Rev.* **2012**, *112*, 2268−2285.
(6) Ge, J.; Yin, Y. *Angew. Chem. Int. Ed.* **2011**, *50*, 1492−1522.
(7) John, S. *Phys. Rev. Lett.* **1987**, *58*, 2486−2489.
(8) Yablonovitch, E. *Phys. Rev. Lett.* **1987**, *58*, 2059−2062.
(9) Marlow, F.; Muldarisnur; Sharifi, P.; Brinkmann, R.; Mendive, C. *Angew. Chem. Int. Ed.* **2009**, *48*, 6212−6233.
(10) Stein, A.; Li, F.; Denny, N. R. *Chem. Mater.* **2008**, *20*, 649−666.
(11) Zhang, J.; Li, Y.; Zhang, X.; Yang, B. *Adv. Mater.* **2010**, *22*, 4249−4269.
(12) Lee, S. Y.; Gradon, L.; Janeczko, S.; Iskandar, F.; Okuyama, K. *ACS Nano* **2010**, *4*, 4717−4724.
(13) Zhao, Q.; Haines, A.; Snoswell, D.; Keplinger, C.; Kaltseis, R.; Bauer, S.; Graz, I.; Denk, R.; Spahn, P.; Hellmann, G.; Baumberg, J. J. *Appl. Phys. Lett.* **2012**, *100*, 101902−4.
(14) Arsenault, A. C.; Puzzo, D. P.; Manners, I.; Ozin, G. A. *Nat. Photonics* **2007**, *1*, 468−472.
(15) Vlad, A.; Frölich, A.; Zebrowski, T.; Dutu, C. A.; Busch, K.; Melinte, S.; Wegener, M.; Huynen, I. *Adv. Funct. Mater.* **2013**, *23*, 1164−1171.
(16) von Freymann, G.; Kitaev, V.; Lotsch, B. V.; Ozin, G. A. *Chem. Soc. Rev.* **2013**, *42*, 2528−2554.
(17) Schäfer, C. G.; Gallei, M.; Zahn, J. T.; Engelhardt, J.; Hellmann, G. P.; Rehahn, M. *Chem. Mater.* **2013**, *25*, 2309−2318.
(18) Galisteo-López, J. F.; Ibisate, M.; Sapienza, R.; Froufe-Pérez, L. S.; Blanco, Á.; López, C. *Adv. Mater.* **2011**, *23*, 30−69.
(19) Ozin, G. A.; Arsenault, A. C. *Mater. Today* **2008**, *11*, 44−51.
(20) You, B.; Shi, L.; Wen, N.; Liu, X.; Wu, L.; Zi, J. *Macromolecules* **2008**, *41*, 6624−6626.
(21) Jiang, P.; Ostojic, G. N.; Narat, R.; Mittleman, D. M.; Colvin, V. L. *Adv. Mater.* **2001**, *13*, 389−393.
(22) Griesebock, B.; Egen, M.; Zentel, R. *Chem. Mater.* **2002**, *14*, 4023−4025.
(23) Li, H.-L.; Marlow, F. *Chem. Mater.* **2006**, *18*, 1803−1810.
(24) Jiang, P.; McFarland, M. J. *J. Am. Chem. Soc.* **2004**, *126*, 13778−13786.
(25) Mihi, A.; Ocaña, M.; Míguez, H. *Adv. Mater.* **2006**, *18*, 2244−2249.
(26) Ruhl, T.; Hellmann, G. P. *Macromol. Chem. Phys.* **2001**, *202*, 3502−3505.
(27) Ruhl, T.; Spahn, P.; Hellmann, G. P. *Polymer* **2003**, *44*, 7625−7634.
(28) Pursiainen, O. L. J.; Baumberg, J. J.; Winkler, H.; Viel, B.; Spahn, P.; Ruhl, T. *Adv. Mater.* **2008**, *20*, 1484−1487.
(29) Ruhl, T.; Spahn, P.; Winkler, H.; Hellmann, G. P. *Macromol. Chem. Phys.* **2004**, *205*, 1385−1393.
(30) Schäfer, C. G.; Smolin, D. A.; Hellmann, G. P.; Gallei, M. *Langmuir* **2013**, *29*, 11275−11283.
(31) Finlayson, C. E.; Spahn, P.; Snoswell, D. R.; Yates, G.; Kontogeorgos, A.; Haines, A. I.; Hellmann, G. P.; Baumberg, J. J. *Adv. Mater.* **2011**, *23*, 1540−15444.
(32) Pursiainen, O. L. J.; Baumberg, J. J.; Ryan, K.; Bauer, J.; Winkler, H.; Viel, B.; Ruhl, T. *Appl. Phys. Lett.* **2005**, *87*, 101902.
(33) Viel, B.; Ruhl, T.; Hellmann, G. P. *Chem. Mater.* **2007**, *19*, 5673−5679.
(34) Haines, A. I.; Finlayson, C. E.; Snoswell, D. R.; Spahn, P.; Hellmann, G. P.; Baumberg, J. J. *Adv. Mater.* **2012**, *24*, OP305−308.
(35) Müller, P.; Wagner, K.; Müller, R.; Quiring, B. *Angew. Makromol. Chem.* **1977**, *65*, 23−39.
(36) Wieczorrek, W.; Lohse, F.; Gempeler, H.; Schneider, W.; Neffgen, B.; Scherzer, W. Polyaddukte. In *Lackharze: Chemie, Eigenschaften und Anwendungen*, 1st ed.; Stoye, D., Freitag, W., Eds.; Carl Hanser Verlag: München, Germany, 1996; pp 183−229.
(37) Wolf, E. Process for the preparation of isocyanate-free uretdiones from isophorone-diisocyanate. U.S. Patent 009 004 301, July 27, 1999.
(38) Wolf, E. Powder coating and its use for thermoresistant substrates. European Patent EP 0780416, June 25, 1997.
(39) Phai, L.; Viollaz, F.; Camberlin, Y.; Lam, T. M.; Pascault, J.-P. *Makromol. Chem.* **1984**, *185*, 281−295.
(40) Wicks, Z. W. *Progr. Org. Coat.* **1975**, *3*, 73−99.
(41) Risch, N.; Westerwelle, U.; Kiene, J.; Keuper, R. *J. Prakt. Chem.* **1999**, *341*, 616−619.
(42) Spahn, P. *PhD Thesis*; Technische Universität Darmstadt, Darmstadt, Germany, 2008
(43) Lorenz, O.; Decker, H.; Rose, G. *Angew. Makromol. Chem.* **1984**, *122*, 83−99.

(44) Cunliffe, A. V.; Davis, A.; Farey, M.; Wright, J. *Polymer* **1984**, *26*, 301−306.
(45) Gerard, J. F.; Perchec, P. L.; Pham, Q. T. *Makromol. Chem.* **1988**, *189*, 1719−1737.
(46) Lomölder, R.; Plogmann, F.; Speier, P. *J. Coat. Technol.* **1997**, *69*, 51−57.
(47) Rochery, M.; Vroman, I.; Lam, T. M. *J. Macromol. Sci., Part A: Pure Appl. Chem.* **2000**, *37*, 259−275.
(48) Holden, G.; Hansen, D. R. Styrenic Thermoplastic Elastomers. In *Thermoplastic Elastomers*, 3rd ed.; Holden, G., Kricheldorf, H. R., Quirk, R. P., Eds.; Carl Hanser Verlag: München, Germany, 2004; pp 45−68.